

# Black holes and nilmanifolds: quasinormal modes as the fingerprints of extra dimensions?

Anna Chrysostomou,<sup>1,2,\*</sup> Alan Cornell,<sup>1,2,†</sup> Aldo Deandrea,<sup>2,‡</sup> Étienne Ligout,<sup>3,§</sup> and Dimitrios Tsimpis<sup>2,¶</sup>

<sup>1</sup>*Department of Physics, University of Johannesburg,  
PO Box 524, Auckland Park 2006, South Africa*

<sup>2</sup>*Institut de Physique des Deux Infinis de Lyon. Université de Lyon, UCBL,  
UMR 5822, CNRS/IN2P3. 4 rue Enrico Fermi, 69622 Villeurbanne Cedex, France.*

<sup>3</sup>*École Normale Supérieure de Lyon, 15 parvis René Descartes, BP 7000, 69342 Lyon Cedex 07, France.*

(Dated: November 17, 2022)

We investigate whether quasinormal modes (QNMs) can be used in the search for signatures of extra dimensions. To address a gap in the Beyond Standard Model (BSM) literature, we focus here on higher dimensions characterised by negative Ricci curvature. As a first step, we consider a product space comprised of a four-dimensional Schwarzschild black hole space-time and a three-dimensional nilmanifold (twisted torus); we model the black hole perturbations as a scalar test field. We find that the extra-dimensional geometry can be stylised in the QNM effective potential as a squared mass-like term. We then compute the corresponding QNM spectrum using three different numerical methods, and determine constraints on this possible extra-dimensional observable from gravitational-wave considerations.

## I. INTRODUCTION

Quasinormal modes (QNMs), the damped and discrete oscillations in space-time that emanate from a perturbed body as it returns to an equilibrium state [1, 2], have served for several decades as a theoretical means of studying  $n$ -dimensional black hole space-times as well as a testing ground for the development of numerical simulations and techniques. Quantum gravity conjectures, modified theories of gravity, stability analyses of naked singularities and novel space-times, the development of numerical relativity simulations, and the explorations of the gauge-gravity duality are but a few of the avenues of research made accessible by black hole QNMs (see Refs. [3–7] for reviews).

From the astrophysical perspective, quasinormal frequencies (QNFs)  $\omega$  lead directly to insights about the nature of their black hole source. Specifically, the oscillation frequency  $\Re\{\omega\}$  and damping  $\tau = -1/\Im\{\omega\}$  of the QNFs are uniquely determined by the characteristic black hole properties of mass  $M$ , spin  $a$ , and charge  $Q$  [8], in accordance with the *no-hair theorem* applicable to final-state black holes [9]. This has earned QNMs the epithet “black hole fingerprints”.

Mathematically, QNMs can be structured as an eigenvalue problem subjected to physically-motivated bound-

ary conditions and dependent strictly on the features of the black hole space-time and the effective potential of the perturbing field. If we consider a static black hole (in an asymptotically-flat space-time) through the classical lens, radiation is purely in-going at the event horizon and purely out-going at spatial infinity; the black hole geometry is characterised solely by its mass [10] while the effective potential depends on the spin of the oscillating field and the multipolar (angular momentum) number  $\ell$ . For each  $\ell$  there are infinitely many overtones  $n$  labelling the QNF in increasing multiples of  $\Im\{\omega\}$ , with the  $n = 0$  *fundamental mode* representing the least-damped and thus longest-lived QNM.

On the basis of spherical symmetry and time independence, the QNM behaviour can be shown to reduce to a simple radial wave equation, as first demonstrated in Refs. [11, 12] for the Schwarzschild case. A wide range of predominantly numerical methods have been developed to determine QNM solutions from such wave equations (see Refs. [6, 7]). Of these, we highlight (i) *inverse-potential methods* that approximate the effective potential with an inverse Pöschl-Teller potential [13] for which bound-state solutions are known to determine the QNF spectrum [14]; (ii) *WKB-based methods* that adapt the semi-classical technique to the QNM problem to compute QNFs in the  $\ell \geq n$  regime [15–17] at sixth-order [18] and beyond (see Ref. [19]); (iii) *photon-orbit methods* such as the inverse multipolar expansion method [20] that harnesses the known link between QNMs and unstable null geodesics [21] to construct an iterative technique to solve the wave-like radial equation with increasing accuracy for large values of  $\ell$  [22].

\* [chrysostomou@ipnl.in2p3.fr](mailto:chrysostomou@ipnl.in2p3.fr)

† [acornell@uj.ac.za](mailto:acornell@uj.ac.za)

‡ [deandrea@ipnl.in2p3.fr](mailto:deandrea@ipnl.in2p3.fr)

§ [etienne.ligout@etu.univ-paris1.fr](mailto:etienne.ligout@etu.univ-paris1.fr)

¶ [tsimpis@ipnl.in2p3.fr](mailto:tsimpis@ipnl.in2p3.fr)

Today, we find ourselves in the unprecedented position wherein we can observe this gravitational radiation. To date, the LIGO-Virgo-KAGRA (LVK) collaboration has confirmed 90 gravitational-wave (GW) events, most of which were the result of a binary black hole collision [23]. The success of the LVK collaboration is a testament to the gravitational waveform modelling expertise, Bayesian statistical analysis techniques, and experimental prowess carefully honed over several decades (see Ref. [24] for the LVK collaboration’s guide on data acquisition and processing, as well as reviews Refs. [5, 25]).

Opportunistically, QNM investigations can now be extended into a new domain, with LVK officially putting general relativity (GR) to the test in the strong regime (for the very first time) and searching for evidence of alternative theories of gravity [26–29]. Furthermore, hopes for the establishment of *black hole spectroscopy* [30] are beginning to be realised [31]: although the  $n = 0$ ,  $\ell = 2$  mode is known to dominate the QNM spectrum, higher harmonics [32] and overtones [33] are being investigated. While it is important to recognise that the post-merger *ringdown* signal is weaker and therefore not always characterisable, the first detected black hole merger event GW150914 [34, 35] was sufficiently loud to accommodate QNM study. We shall restrict our discussion to this event within this work, unless otherwise stated.

However, the establishment of GW astronomy as a new cosmological probe promises opportunities for searches of new physics, with GWs acting as a complementary laboratory to collider physics experiments [36–38]. Most of these are predicated on whether an electroweak phase transition within a particle physics model can be a strong enough first order transition, such that its corresponding stochastic GW signal lies within the sensitivity range of present or future GW detectors. As successfully demonstrated in Ref. [39], models based at scales of Grand Unified Theories can be good candidates for detection.

Here, we shall focus specifically on the prospects of detecting evidence of extra dimensions. Search strategies for signatures of extra dimensions in GWs are already being investigated in the literature (see Refs. [40–42]). The compact extra dimensions considered feature a variety of different geometries (Ricci-flat [43–45], toroidal [46], warped toroidal [47] extra dimensions, etc.). These have so far predicted GWs whose frequencies are of the order of  $10^{12} - 10^{14}$  Hz, far exceeding the  $10^3 - 10^4$  Hz upper limit of present and planned detectors [48, 49].

This begs the question: could alternate geometries lead to successful GW detection? In the following, we shall consider a particularly simple setup: a direct product space featuring a four-dimensional (4D) Minkowski space-time and a three-dimensional (3D) negative space

$\mathcal{M}_4 \times \mathcal{N}_3$ . This higher-dimensional component is comprised of a twisted torus – known as a *nilmanifold* – constructed from the non-trivial fibrations of layered tori. The nilmanifold is one of the few geometries that allows for analytic calculations of mass spectra and Kaluza-Klein reductions, and boasts a number of phenomenologically-interesting properties that we shall discuss in section II A.

To perform this search, we turn to ringdown data from binary black hole collisions, rather than stochastic GWs. In fact, there have already been considerations for extra dimensions using black hole QNMs. These, however, are concentrated on the five-dimensional (5D) Randall-Sundrum II [50] model: through the formalism of Shiromizu *et al.* [51] and Dadhich *et al.*, a 4D effective framework can be established from a 5D general relativity construction, leading to a (neutral) black hole solution that resembles the (charged) Reissner-Nordström metric. The so-called *tidal charge*  $\beta = Q^2/(4M^2)$  is a manifestation of the influence of the extra dimension. In Ref. [52], this is the observable utilised to constrain extra dimensions, but is found to disfavour extra dimensions.

It is not clear how to extend the Shiromizu *et al.* formalism to the partially-compactified geometry we wish to analyse here, nor is it obvious whether this tidal charge observable can be probed. Bearing these points in mind, we propose a new setup that exploits the variable-separable nature of our extra-dimensional space-time and the QNM problem we consider: we employ a Kaluza-Klein reduction to contain the extra-dimensional behaviour into a mass-like term that can be incorporated into the QNM effective potential. We shall demonstrate how this enables the application of QNM literature on massive oscillating fields, as well as studies on parametric deviations from GR employed by the LVK collaboration.

In section II, we define the “Schwarzschild-nilmanifold” setup we investigate: we outline the interesting features and the construction of the nilmanifold, as well as the construction of the partially-compactified seven-dimensional (7D) metric and the scalar field<sup>1</sup> we use to explore it. There, we shall derive a 4D effective potential in which the higher-dimensional character is encoded in an effective mass term. In so doing, we recreate the problem of massive scalar QNMs: a scenario that has been used as a case study for numerical development in the QNM literature.

In section III, we compute the QNF spectrum using

---

<sup>1</sup> It is standard practice in QNM studies to explore uncharted space-times and/or novel techniques with scalar test fields to test for feasibility.

the three numerical methods mentioned, *viz.* the inverse Pöschl-Teller potential method, the WKB method, and the inverse- $\ell$  method. We include also a discussion on how the QNF spectrum is affected by the mass-like term. In this way, we shall determine an upper bound under which detectable black hole QNMs may serve as an appropriate probe for extra dimensions in this construction. To constrain this mass-like parameter further, we introduce bounds from studies on the parametric deviation of GW data from GR predictions, using the most stringent results published by the LVK collaboration [29]. This step shall be carried out in section IV. By comparing the magnitude of the deviation from GR in the ringdown phase with the deviations in a the QNF spectrum caused by our introduction of the effective mass term, we are able to place naïve constraints on detectable QNFs harbouring extra-dimensional signatures. While our interest lies specifically in the case of negative extra-dimensional components, this result is agnostic to the extra-dimensional scalar curvature. We note, however, that our objective here is not to supply a definitive constraint on extra dimensions, but rather to introduce a possible road-map for consideration.

## II. A SCHWARZSCHILD-NILMANIFOLD EXTRA-DIMENSIONAL SETUP

Compact negative spaces (i.e. spaces with negative Ricci scalar curvature) have been interrogated extensively within the mathematical literature [53, 54]. Among members of the string theory community, a burgeoning interest in such spaces is developing in the wake of a recent observation that negatively-curved manifolds are a requirement for classical de Sitter solutions with orientifold planes [55–57]. In the context of particle physics, extra-dimensional models characterised by partial or total negative scalar curvature remain comparatively under-explored.

Phenomenologically, studies on compact hyperbolic spaces are promising for their capacity to include cosmological observations such as homogeneity and flatness [58–60]. Moreover, these models could be used to address the hierarchy problem between the Planck and the electroweak scale by virtue of their geometrical properties. Compact negative spaces possess two characteristic length scales:  $\ell_c$ , associated with local properties like the curvature and fixed by the equations of motion, and  $\ell_G$ , associated with global properties like the volume and independent of the equations of motion. Their volume grows exponentially with  $\ell_c/\ell_G$ , leading to an exponential reduction of the Planck length, which in turn yields

a natural explanation for the perceived discrepancy in energy scales [61]. Furthermore, the Kaluza-Klein mass spectra associated with such spaces are usually similar to those of Randall-Sundrum models [62] in that they accommodate the electroweak-Planck scale hierarchy without introducing light Kaluza-Klein modes [61].

Motivated by these implications, a series of investigations [63–67] have focused model-building efforts on a compact, negatively-curved manifold whose tangent vectors form a Lie algebra that is nilpotent *viz.* a nilmanifold  $\mathcal{N}_3$  (see Refs. [68, 69]). In the sections that follow, we shall outline how the nilmanifold is constructed from the Heisenberg algebra and demonstrate the Kaluza-Klein expansion of a scalar field in this context, as established in Ref. [63]. With these elements in place, we may proceed to the construction of our Schwarzschild-nilmanifold setup, and the Kaluza-Klein reduction that allows us to treat the oscillations travelling through the 7D product space-time as a massive 4D scalar field.

### A. Algebra, geometry, and a 3D scalar field

Any Lie group of dimension  $d$  can be understood as a  $d$ -dimensional differentiable manifold. Under certain conditions (see Ref. [70] for a review), a solvable<sup>2</sup> Lie group  $G$  can be divided by a lattice  $\Gamma$ , a discrete subgroup of  $G$ , to construct a compact solvmanifold (i.e. a twisted torus) by means of discrete identifications [71]. *Nilpotent*<sup>3</sup> groups are a special subclass of solvable groups. For them, the compactness criterion requires the structure constants to be rational in some basis [72]. We refer to their corresponding compact manifolds as *nilmanifolds*.

Consider the  $d$ -dimensional Lie algebra  $\mathfrak{g}$  generated by the vectors  $\{Z_a, a = 1, \dots, d\}$  satisfying

$$[Z_b, Z_c] = f^a_{bc} Z_a. \quad (2.1)$$

Here, the structure constants satisfy  $f^a_{bc} = -f^a_{cb}$ . The corresponding  $d$ -dimensional manifold admits a globally-defined orthonormal frame  $\{e^a, a = 1, \dots, d\}$  (where this basis defines the dual space of one-forms  $\mathfrak{g}^*$ ). This frame obeys the Maurer-Cartan equation

$$de^a = -\frac{1}{2} f^a_{bc} e^b \wedge e^c = -\sum_{b < c} f^a_{bc} e^b \wedge e^c, \quad (2.2)$$

<sup>2</sup> A Lie group  $G$  is solvable if its Lie algebra  $\mathfrak{g}$  terminates in the null algebra i.e. the sequence  $\mathfrak{g}_0 = \mathfrak{g}$ ,  $\mathfrak{g}_{n+1} = [\mathfrak{g}_n, \mathfrak{g}_n]$  for  $n \geq 0$  reduces to the null algebra after a finite number of steps.

<sup>3</sup> A Lie group  $G$  is nilpotent if the sequence  $\mathfrak{g}_{n+1} = [\mathfrak{g}, \mathfrak{g}_n]$  reduces to the null algebra after a finite number of steps.

with the exterior derivative  $d$ . Since the dual space  $\mathfrak{g}^* \approx T_e G^*$ ,  $\{e^a, a = 1, \dots, d\}$  provides – by left invariance – a basis for the cotangent space  $T_x G^*$  at every point  $x \in G$ , the one-forms are globally defined on the manifold. These one-forms will have their non-trivial identification through the “lattice action” when  $G$  is divided by  $\Gamma$ . Note that  $f^a_{bc}$  is related to the spin connection.

In flat indices and for a unimodular Lie algebra, the Ricci tensor is given by

$$\mathcal{R}_{cd} = \frac{1}{2} \left( -f^b_{ac} f^a_{bd} - \delta^{bg} \delta_{ah} f^h_{gc} f^a_{bd} + \frac{1}{2} \delta^{ah} \delta^{bj} \delta_{ci} \delta_{dg} f^i_{aj} f^g_{hb} \right), \quad (2.3)$$

with  $\delta_{ab}$  serving as a Euclidean metric. For the nilpotent algebra, and thus for the nilmanifold case, the first term vanishes. The Ricci tensor is thus nowhere-vanishing and the corresponding Ricci scalar emerges as

$$\mathcal{R} = -\frac{1}{4} \delta_{ad} \delta^{bc} \delta^{cg} f^a_{bc} f^d_{cg}. \quad (2.4)$$

The Ricci scalar is strictly negative.

From Eq. (2.2), we can see that  $d = 3$  is the lowest dimensionality for which this expression is non-trivially satisfied. For  $d = 3$ , there is the trivial Abelian algebra that leads to a three-torus, as well as three different solvable algebras. Of these, one is nilpotent: the *Heisenberg* algebra

$$[Z_1, Z_2] = -\mathbf{f} Z_3, \quad [Z_1, Z_3] = [Z_2, Z_3] = 0, \quad (2.5)$$

with  $\mathbf{f} = -f^3_{12} \neq 0$  such that the Maurer-Cartan equation becomes

$$de^3 = \mathbf{f} e^1 \wedge e^2, \quad de^1 = 0, \quad de^2 = 0. \quad (2.6)$$

The only nonzero structure constant  $\mathbf{f} = -f^3_{12} \in \mathbb{R}$  is the *geometric flux* serving as the nilmanifold’s *twist parameter*. The corresponding geometric properties of the nilmanifold can be relayed through the Maurer-Cartan equation,

$$de^3 = \mathbf{f} e^1 \wedge e^2, \quad de^1 = 0, \quad de^2 = 0, \quad (2.7)$$

from which we define

$$e^1 = r^1 dy^1, \quad e^2 = r^2 dy^2, \quad e^3 = r^3 (dy^3 + N y^1 dy^2) \quad (2.8)$$

for the constant radii  $r^{1,2,3} > 0$ , angular coordinates  $y^m \in [0, 1]$ , and the integer  $N = r^1 r^2 \mathbf{f} / r^3$  [63].

The discrete identifications that make the compactifi-

cation possible are

$$y^1 \sim y^1 + n^1, \quad y^2 \sim y^2 + n^2, \quad y^3 \sim y^3 + n^3 - n^1 N y^2, \quad (2.9)$$

for  $n^{m=1,2,3} \in [0, 1]$ . In other words, these identifications correspond to the lattice action responsible for establishing  $\mathcal{N}_3$  as a nilmanifold. Eq. (2.9) leaves Eq. (2.8) invariant.

In this way, the compact manifold is fully characterised as a twisted  $S^1$  fibration over layered tori  $T^2$ . The twist is along the fibre coordinate  $y^3$ , while the base is parameterised by the coordinates  $(y^1, y^2)$ . Physically,  $y^{m=1,2,3}$  are angles defined on  $[0, 1]$ . The constant radii  $r^m$  have units of length, the coordinates  $y^m$  are dimensionless, and  $\mathbf{f}$  has units of inverse length (i.e. energy).

The most general left-invariant metric for the nilmanifold is given by

$$ds^2 = \delta_{ab} E^a E^b, \quad E^a = (L^{-1})^a_b e^b, \quad (2.10)$$

where we use  $E^a$  to denote the one-forms related to the orthonormal basis  $e^a$  through the constant  $GL(3, \mathbb{R})$  transformation  $L$ .

To demonstrate the construction of the scalar mass spectrum, we shall consider the simplified special case in which  $r^m = 1$  and  $\mathbf{f} = 1$ . The nilmanifold metric then becomes

$$ds^2_{\text{nil}} = \delta_{ab} e^a e^b = (dy^1)^2 + (dy^2)^2 + (dy^3 + y^1 dy^2)^2. \quad (2.11)$$

To understand the behaviour of a scalar field on this space, we consider the massive Klein-Gordon equation. Let us begin with the Laplacian

$$\nabla^2 \Phi = \frac{1}{\sqrt{g}} \delta_m (\sqrt{g} g^{mn} \delta_n \Phi), \quad (2.12)$$

where the determinant  $\sqrt{g} = r^1 r^2 r^2$  reduces to 1 in our simplified metric. We may write

$$\nabla^2 u = \left( \partial_1^2 + (\partial_2 - y^1 \partial_3)^2 + \partial_3^2 \right) u, \quad (2.13)$$

as we shall consider the expansion of  $u$  on the space of functions invariant under Eq. (2.9), beginning with the functions depending only on the base coordinates  $(y^1, y^2)$ . In this case, the Laplacian is easily diagonalised:

$$(\nabla^2 + \mu_{\beta, \gamma}^2) \tilde{v}_{\beta, \gamma} = 0, \quad (2.14)$$

where we define

$$\tilde{v}_{\beta, \gamma}(y^1, y^2) = e^{2\pi i \beta y^1} e^{2\pi i \gamma y^2}, \quad (2.15)$$

for  $\beta, \gamma \in \mathbb{Z}$ , as invariant under Eq. (2.9), and the Klein-Gordon masses as

$$\mu_{\beta, \gamma}^2 = 4\pi^2 (\beta^2 + \gamma^2). \quad (2.16)$$

We can present a more generalised expression using the *Weil-Brezin-Zak* transforms [73] for a basis of invariant functions  $u_{\kappa, \lambda}$ ,

$$u_{\kappa, \lambda}(y^1, y^2, y^3) = e^{2\pi\kappa i(y^3 + y^1 y^2)} e^{2\pi\lambda i y^1} \times \sum_{\sigma} e^{2\pi\kappa\sigma i y^1} f(y^2 + \sigma), \quad (2.17)$$

for  $\kappa, \lambda, \sigma \in \mathbb{Z}$ . Since  $u_{\kappa, \lambda}$  is invariant under Eq. (2.9) for all values of  $f(x)$ , the functions remain well-defined across our nilmanifold  $\mathcal{N}_3$ . Upon substituting Eq. (2.17) into Eq. (2.13), we obtain

$$\nabla^2 u_{\kappa, \lambda} = e^{2\pi\kappa i(y^3 + y^1 y^2)} e^{2\pi\lambda i y^1} \sum_{\sigma} e^{2\pi\kappa\sigma i y^1} \times [\partial_z^2 - 4\pi^2 (\kappa^2 + (\kappa(y^2 + \sigma) + \lambda)^2)] f(y^2 + \sigma), \quad (2.18)$$

where we require that  $\kappa \neq 0$  to retain the  $y^3$ -dependent terms.

If we introduce  $z_{\sigma} = y^2 + \sigma + \lambda/\kappa$  and  $g(z_{\sigma}) = f(y^2 + \sigma)$ , we can rewrite the above Laplacian as

$$\nabla^2 u_{\kappa, \lambda} = e^{2\pi\kappa i(y^3 + y^1 y^2)} e^{2\pi\lambda i y^1} \sum_{\sigma} e^{2\pi\kappa\sigma i y^1} \times [\partial_{z_{\sigma}}^2 - (2\pi\kappa)^2 (z_{\sigma}^2 + 1)] g(z_{\sigma}^2 + 1). \quad (2.19)$$

From the normalised Hermite functions

$$X_{\nu}(z) = e^{-z^2/2} H_{\nu}(z), \quad \nu \in \mathbb{N}, \quad (2.20)$$

where  $H_{\nu}$  represents the Hermite polynomials, we may define

$$X_{\nu}^{\rho}(z) = |\rho|^{1/4} X_{\nu}(|\rho|^{1/2} z) \quad (2.21)$$

for  $\rho \in \mathbb{R}^*$  [73]. By the properties of Hermite polynomials, Eq. (2.21) satisfies the differential equation

$$(\partial_z^2 - \rho^2 z^2) X_{\nu}^{\rho}(z) = -(2\nu + 1) |\rho| X_{\nu}^{\rho}(z). \quad (2.22)$$

With the insertion of  $g(z_{\sigma} = X_{\nu}^{2\pi\kappa}(z_{\sigma}))$  into Eq. (2.19), we obtain the 3D Klein-Gordon equation

$$(\nabla^2 + M_{\kappa, \lambda, \nu}^2) \tilde{u}_{\kappa, \lambda, \nu} = 0, \quad (2.23)$$

where the masses and wavefunctions are, respectively,

$$M_{\kappa, \lambda, \nu}^2 = (2\pi\kappa)^2 \left( 1 + \frac{2\nu + 1}{2\pi|\kappa|} \right), \quad (2.24)$$

$$\tilde{u}_{\kappa, \lambda, \nu}(y^1, y^2, y^3) = e^{2\pi\kappa i(y^3 + y^1 y^2)} e^{2\pi\lambda i y^1} \sum_{\sigma} e^{2\pi\kappa\sigma i y^1} \times X_{\nu}^{2\pi\kappa} \left( y^2 + \sigma + \frac{\lambda}{\kappa} \right) \quad (2.25)$$

for  $\sigma \in \mathbb{Z}$ ,  $\nu \in \mathbb{N}$ ,  $\kappa \in \mathbb{Z}^*$ , and  $\lambda = 0, \dots, |\kappa| - 1$ . The range of  $\lambda$  is derived from the fact that  $\lambda$  itself is defined modulo  $\kappa$ , which in turn is a consequence of the identity

$$\tilde{u}_{\kappa, \lambda + \kappa\tau, \nu}(y^1, y^2, y^3) = \tilde{u}_{\kappa, \lambda, \nu}(y^1, y^2, y^3) \quad \forall \tau \in \mathbb{Z}. \quad (2.26)$$

By virtue of Eq. (2.24)'s independence of  $\lambda$ , there exists a mass degeneracy. The wavefunctions are parameterised by a finite number of inequivalent values of  $\lambda$  such that the level of the degeneracy is  $|\kappa|$ . Note that only one zero-mode (i.e. with vanishing mass) exists for this Klein-Gordon equation,  $\tilde{v}_{0,0}$ , corresponding to the modes of the torus base.

We conclude this discussion on the nilmanifold space with the physical spectrum associated with a scalar field propagating on  $\mathcal{N}_3$ . This is achieved by reintroducing dimensional parameters  $r^m$  and  $\mathbf{f}$  [63]. We may distinguish between *torus modes*,

$$v_{\beta, \gamma}(y^1, y^2) = \frac{1}{\sqrt{V}} e^{2\pi i \beta y^1} e^{2\pi i \gamma y^2}, \quad (2.27)$$

$$\mu_{\beta, \gamma}^2 = \beta^2 \left( \frac{2\pi}{r^1} \right)^2 + \gamma^2 \left( \frac{2\pi}{r^2} \right)^2, \quad (2.28)$$

and *fibre modes*,

$$u_{\kappa, \lambda, \nu}(y^1, y^2, y^3) = \sqrt{\frac{r^2}{|N|V}} \frac{1}{\sqrt{2^{\nu} \nu! \sqrt{\pi}}} e^{2\pi\kappa i(y^3 + N y^1 y^2)} \times e^{2\pi\lambda i y^1} \sum_{\sigma} e^{2\pi\kappa\sigma i y^1} X_{\nu}^{\rho}(w_{\sigma}), \quad (2.29)$$

$$M_{\kappa, \lambda, \nu}^2 = \kappa^2 \left( \frac{2\pi}{r^3} \right)^2 + (2\nu + 1) |\kappa| \frac{2\pi \mathbf{f}}{r^3}, \quad (2.30)$$

for which we define

$$\rho = \frac{2\pi \mathbf{f}}{r^3} \kappa, \quad w_{\sigma} = r^2 \left( y^2 + \frac{\sigma}{N} + \frac{\lambda}{N\kappa} \right),$$

and the volume

$$V = \int d^3 y \sqrt{g} = r^1 r^2 r^3. \quad (2.31)$$

The scalar spectrum on the nilmanifold contains a complete tower of modes on the torus that is independent of the fibre coordinate and radius. The fibre modes, whose mass spectrum is a function of the radial components and the curvature-related energy scale  $\mathbf{f}$ , have been shown to be tunable in Ref. [63] by varying parameters in the generalised case; the fibre modes can be made

lighter than their toroidal counterparts and the energy gaps in the spectrum may be enhanced. From the structure of Eq. (2.30) itself, we understand that the fibre modes present with a unique mass spectrum: the typical  $1/R$  Kaluza-Klein term is augmented by the  $\mathbf{f}$  term that enforces more finely-spaced modes that follow a linear Regge trajectory. This suggests that the fibre modes may lead to a unique collider signature, and should be the focus of searches for nilmanifold extra-dimensional frameworks.

## B. A Schwarzschild black hole and its scalar QNM

GR remains our most complete theory of gravity to date. Its underlying principle is the relationship it defines between the geometry and matter content of a space-time, expressed concisely through the Einstein field equations,

$$G_{\mu\nu} + \Lambda g_{\mu\nu} = \kappa T_{\mu\nu} . \quad (2.32)$$

Here, the Einstein tensor  $G_{\mu\nu}$  expresses the local space-time curvature,  $\kappa$  is the Einstein gravitational constant, and  $T_{\mu\nu}$  is the stress-energy tensor that defines the energy, momentum, and stress for the matter and field content within the local space-time [9]. We set  $G = c = 1$ , unless otherwise stated. In asymptotically-flat space-times, the cosmological constant  $\Lambda$  vanishes. To describe the evolution of the metric and the fields, we utilise the Einstein-Hilbert gravitational action

$$S = \frac{1}{16\pi G} \int d^4x \sqrt{-g} (R + \mathcal{L}_m) , \quad (2.33)$$

where we use  $\mathcal{L}_m$  to refer to all matter fields  $\Psi$  within the space-time, and whose stress, energy, and momentum are encompassed by  $T_{\mu\nu}$ .

Within the context of GR, Birkhoff's theorem stipulates that the most general spherically-symmetric vacuum solution of Eq. (2.32) is the Schwarzschild metric

$$ds_{\text{BH}}^2 = g_{\mu\nu}^{\text{BH}} dx^\mu dx^\nu = -f(r) dt^2 + f(r)^{-1} dr^2 + r^2(d\theta^2 + \sin^2\theta d\phi^2) , \quad (2.34)$$

where  $f(r) = 1 - r_H/r$  and  $r_H = 2M$  is the Schwarzschild event horizon. For such a black hole, the length scale is defined by  $M = mGc^{-2}$  for black hole mass  $m^{\text{BH}}$  [74], and is set to unity. The Schwarzschild coordinates  $(t, r, \theta, \phi)$  are defined on the regions  $t \in (-\infty, +\infty)$ ,  $r \in (r_H, +\infty)$ ,  $\theta \in (0, \pi)$ , and  $\phi \in (0, 2\pi)$ ; the tortoise coordinate  $dr_* = dr/f(r)$  can be introduced to map the semi-infinite region of  $(r_H, +\infty)$  to  $(-\infty, +\infty)$ .

Eq. (2.34) describes an isolated, static, and neutral 4D black hole [9, 75] that is fully characterised by its mass  $M$  [10]. Mathematically, black holes are therefore simple objects: they are pure geometry and do not require an equation of state to describe their evolution. Astrophysical black holes, however, are perpetually in a perturbed state: even if somehow isolated from the fields and matter in their immediate vicinity, they interact with the surrounding vacuum through Hawking radiation [76].

Black hole perturbation theory therefore considers a linearised approximation in which the black hole is described using

$$g'_{\mu\nu} = g_{\mu\nu}^{\text{BH}} + \delta_{\mu\nu} , \quad (2.35)$$

where the unperturbed black hole metric  $g_{\mu\nu}^{\text{BH}}$  is referred to as the ‘‘background’’ and the ‘‘perturbations’’  $\delta_{\mu\nu}$  are considered to be very small ( $\delta_{\mu\nu} \ll g_{\mu\nu}^{\text{BH}}$ ). Similarly, we may consider a perturbed background field  $\Psi' = \Psi^{\text{BG}} + \psi$ . We may then substitute  $g'_{\mu\nu}$  and  $\Psi'$  into Eq. (2.32), linearise the system of equations with respect to  $\delta_{\mu\nu}$  and  $\psi$ , and thereby deduce the linearised set of differential equations satisfied by the perturbations.

As detailed in Chandrasekhar's book [75], black hole QNM behaviour within a classical GR context can be inferred by substituting the perturbed metric, Eq. (2.35) and an ansatz into the Einstein field equations, and then solving for the vacuum solution under the physically-motivated QNM boundary conditions.<sup>4</sup> The QNM ansatz and the number of ordinary differential equations required to describe the QNM propagation are derived from the symmetries of the background space-time: in the Schwarzschild case (static, non-rotating, and spherically-symmetric), the wave-function is written in variable-separable form,

$$\Phi_{n\ell m}^s(\mathbf{x}) = \sum_n \sum_{\ell, m} \frac{\psi_{sn\ell}(r)}{r} Y_{m\ell}^s(\theta, \phi) , \quad (2.36)$$

and the angular behaviour is relayed through spherical harmonics

$$\nabla^2 Y_{m\ell}^s(\theta, \phi) = -\frac{\ell(\ell+1)}{r^2} Y_{m\ell}^s(\theta, \phi) . \quad (2.37)$$

Since the black hole is static, the corresponding ordinary differential equations are time independent. Con-

<sup>4</sup> As stipulated in Ref. [7], at sufficiently late times, the QNMs obtained through this linear approximation remain in good agreement with those calculated via the full nonlinear integration of the Einstein equations [77, 78].

sequently, the defining QNM behaviour is then fully encapsulated by the radial component.

As a simple example that retains the physical implications, we can consider Eq. (2.36) to be a scalar test field evolving on a fixed background in vacuum that contributes negligibly to the energy-density of the system. Explicitly, we may focus on the second term of Eq. (2.33), which becomes

$$\mathcal{L}_m = -(\partial_\mu \Psi)^\dagger \partial^\mu \Psi \quad (2.38)$$

for a minimally-coupled massless scalar field. The equations of motion satisfied by the fields  $g_{\mu\nu}$  and  $\Psi$  are then the massless Klein-Gordon equation for a curved space-time,

$$\nabla_\mu \nabla^\mu \Psi = \frac{1}{\sqrt{-g}} \partial_\mu (\sqrt{-g} g^{\mu\nu} \partial_\nu \Psi) = 0 \quad (2.39)$$

and Eq. (2.32), with  $T_{\mu\nu}$  quadratic in  $\Psi$ . In this context, the linearised equations of motion for  $\psi$  and  $\delta_{\mu\nu}$  decouple when  $\Psi^{\text{BG}} = 0$ , allowing for the metric fluctuations  $\delta_{\mu\nu}$  to be set to zero. With the substitution of Eq. (2.36) into the above equation and the application of the tortoise coordinate, we obtain the radial wave-like equation sufficient to convey the QNM behaviour

$$\frac{d^2 \psi}{dr_*^2} + (\omega^2 - V(r)) \psi = 0, \quad (2.40)$$

where

$$V(r) = f(r) \left( \frac{\ell(\ell+1)}{r^2} + \frac{f'(r)}{r} \right). \quad (2.41)$$

### C. The effective 4D QNM problem

In combining Eqs. (2.34) and (2.11), we can construct our extra-dimensional manifold  $ds_{7D}^2 = ds_{\text{BH}}^2 + ds_{\text{nil}}^2$ . In the absence of mixing terms, we consider a 7D scalar field propagating on this direct product space to be expressible as

$$\Psi_{n\ell m}^s(\mathbf{z}) = \sum_{n=0}^{\infty} \sum_{\ell, m}^{\infty} \frac{\psi_{sn\ell}(r)}{r} Y_{m\ell}^s(\theta, \phi) Z(y^1, y^2, y^3) e^{-i\omega t}. \quad (2.42)$$

To determine the QNM behaviour, we have shown that we may use the Klein-Gordon equation. Recall that the Laplacian of a product space is the sum of its parts, such that

$$\nabla^2 \Psi(\mathbf{z}) = (\nabla_{\text{BH}}^2 + \nabla_{\text{nil}}^2) \Phi_{n\ell m}^s(\mathbf{x}) Z(\mathbf{y}). \quad (2.43)$$

However, if we choose to impose a Kaluza-Klein reduction, we may encode the higher-dimensional behaviour through an effective mass term representing a Kaluza-Klein tower of states. This allows us to formulate the 7D scalar field evolution as a 4D “massive” Klein-Gordon equation,

$$\frac{1}{\sqrt{-g}} \partial_\mu (\sqrt{-g} g^{\mu\nu} \partial_\nu \Psi) - \mu^2 \Psi = 0, \quad (2.44)$$

where

$$\nabla_{\text{nil}}^2 Z(\mathbf{y}) = -\mu^2 Z(y^1, y^2, y^3). \quad (2.45)$$

Using the derivative of the tortoise coordinate  $dr_* = dr/f(r)$ , we extract the radial component of the QNM to produce a characteristic wave-like equation containing the QNF and the effective scalar potential,

$$\frac{d^2 \psi}{dr_*^2} + (\omega^2 - V(r)) \psi = 0, \quad (2.46)$$

where

$$V(r) = \left( 1 - \frac{2M}{r} \right) \left( \frac{\ell(\ell+1)}{r^2} + \frac{2M}{r^3} + \mu^2 \right). \quad (2.47)$$

Within the QNM literature, a Klein-Gordon equation with a non-vanishing mass<sup>5</sup> has been used to describe the behaviour of massive 4D scalar QNMs in a black hole space-time [19, 79–84]. The reduction of our Schwarzschild-nilmanifold QNM equation to Eq. (2.46) allows us to draw upon known computational techniques and behaviours to constrain  $\mu$ . In the next section, we shall discuss the methods we employ here to compute the QNF spectrum from Eq. (2.46), after which we shall comment on the effect of  $\mu$  on the QNFs and the implication thereof.

## III. THE QNF SPECTRUM FOR THE SCHWARZSCHILD-NILMANIFOLD SETUP

### A. Computing the QNFs

There are few techniques established within the QNM literature that generate exact solutions for QNFs. This is due in part to the technical challenges introduced by the inherently dissipative nature of the QNM problem. Since radiation is irrevocably lost at spatial infinity and

<sup>5</sup> It is worth noting that the origin and nature of this mass is rarely discussed in the context of QNMs.

at the event horizon, the system is not time-symmetric; the eigenvalue problem is consequentially non-Hermitian and the eigenvalues are complex. In general, the corresponding eigenfunctions are then not normalisable and do not form a complete set (see reviews [3, 6, 7] for further discussion). To circumvent this problem, a method was developed in Refs. [14, 85, 86] that exploits the relationship between the QNMs of a potential barrier and the bound states of the inverted potential [14], as explained in the introduction. The procedure involves fitting the effective QNM potential featured in Eq. (2.46) to a well-understood substitute (characterised by exponential decay and other key common features) for which analytic solutions are known. In the case of several black hole space-times<sup>6</sup>, the Pöschl-Teller potential [13] can serve as the inverted effective potential and the QNF spectrum is extracted from the bound-state solutions.

However, physically-motivated numerical methods remain a popular alternative. For a spherically-symmetric black hole, QNMs can be treated as waves trapped on the photon sphere<sup>7</sup>, albeit gradually “leaking out” [21]. In Refs. [15–17], this scenario was interpreted as a scattering problem, where the effective QNM potential serves as a potential barrier that tends to constant values in the opposing asymptotic limits. From this framing, a modified WKB method was developed that exploited the Bohr-Sommerfeld quantisation condition of quantum mechanics to establish a semi-analytical technique to compute black hole QNFs.

The WKB formula involves the matching of asymptotic solutions across two turning points that are the roots of the effective QNM potential. With the aid of a Taylor expansion about the peak of the potential barrier  $x = r_0$ , it becomes possible to relate the ingoing and outgoing solutions of the wave-like Eq. (2.46) and thereby obtain an expression for the QNFs and their wave-function. At lowest order [15], this WKB method yields

$$\omega^2(\ell, n) \approx V(r_0) - i(n + 1/2)\sqrt{-2V''(r_0)}, \quad (3.48)$$

where derivatives with respect to  $r$  are denoted by primes and  $r_0$  represents the peak of the potential. From this

<sup>6</sup> While the use of the inverted Pöschl-Teller potential leads to the production of QNFs with errors  $> 1\%$  for Schwarzschild black holes with  $\ell > 2$ , greater accuracy can be found for Schwarzschild-de Sitter and Reissner-Nordström-de Sitter black hole space-times, against which the Pöschl-Teller potential exactly matches.

<sup>7</sup> The photon sphere of a non-rotating, spherically-symmetric black hole is comprised of circular null geodesics of fixed radius  $r_c$ . QNM behaviour can be compared with the photons orbiting this sphere:  $\text{Re}\{\omega\}$  serves as the angular velocity while  $\text{Im}\{\omega\}$  refers to the instability timescale of the photon orbit.

simple expression alone, the dominant QNMs for a  $s = 2$  perturbing field may be computed with an accuracy of 6% [16]; at third-order [17], the accuracy improves to fractions of a percent [19]. While the WKB method is far more successful than we would expect [87], it is understood that this method produces more accurate results for QNFs when  $\ell \gtrsim 2$  at lower orders [88]. However, even at higher orders (i.e. see the 12th-order WKB method established in Refs. [89, 90]), the method still works best for  $\ell > n$ , with further accuracy found at higher multipolar values. For low values of  $n$ , Eq. (3.48) demonstrates that the QNF can be closely determined by the height of its associated potential barrier, as well as its second derivative.

There are, however, known limitations to the use of this modified WKB method: as reviewed in Ref. [19], care must be taken when applying the technique to instability analyses and contexts with large overtones, effective potentials with non-constant asymptotics, space-times with higher dimensions, QNMs of massive perturbing fields, etc. Specifically, in the case of massive scalar fields – the QNM context which aligns most closely with our setup here – the  $\mu^2$  term in the effective potential produces an additional turning point beyond the two over which the WKB matching is traditionally applied. This becomes significant for large values of  $\mu$ , as the local minimum is lost [80]. Physically, at a sufficiently large mass, the fields approach the *quasiresonance regime*, at which point the the amplitudes in the asymptotic regions approach zero and the application of the WKB method is no longer feasible; damping becomes minimal, such that the modes become purely real and arbitrarily long-lived.

To compute highly massive QNMs most accurately, one would have to take into account the minimum emergent on the right side of the peak and the consequent backscattering from that barrier. However, this is not strictly necessary provided the peak lies above the value to which the effective potential asymptotes i.e.  $\mu^2 \leq V(r_0)$  (see section VI B of Ref. [19] for explicit comparisons).

Recently, a numerical method was put forth in Ref. [20] that returns to the intuitive picture proposed by Goebel [21]. Using a novel ansatz for Eq. (2.46) derived from the equations of motion for a test particle following the null geodesic of a spherically-symmetric black hole, Dolan and Ottewill iteratively construct a series expansion in inverse powers of  $L = \ell + 1/2$  for the QNF,

$$\omega = \sum_{k=-1}^{\infty} \omega_k L^{-k}. \quad (3.49)$$

We have studied this technique extensively within the

TABLE I: QNFs for  $n = 0$  and  $\ell = 2$  for  $0.0 \leq \mu \leq 0.7$  using the WKB at  $\mathcal{O}(V^6)$ , Pöschl-Teller (PT) method, and Dolan-Ottewill (DO) expansion at  $\mathcal{O}(L^{-6})$ .

$\mu$	$\omega$ (WKB)	$\omega$ (PT)	$\omega$ (DO)
0.0	0.4836-0.0968 i	0.4874-0.0979 i	0.4836- 0.0968i
0.1	0.4868-0.0957 i	0.4909-0.0968 i	0.4868 - 0.0957i
0.2	0.4963-0.0924 i	0.5015-0.0936 i	0.4963 - 0.0924i
0.3	0.5123-0.0868 i	0.5192-0.0881 i	0.5124 - 0.0868i
0.4	0.5351-0.0787 i	0.5443-0.0800 i	0.5352 - 0.0787i
0.5	0.5649-0.0676 i	0.5770-0.0690 i	0.5653 - 0.0676i
0.6	0.6022-0.0528 i	0.6181-0.0541 i	0.6032 - 0.0532i
0.7	0.1396+0.2763 i	0.6695-0.0312 i	0.6500 - 0.0343i

eikonal limit in Ref. [22]; here, we find that the QNF emerges as a function of both  $L$  and  $\mu$  when the method of Ref. [20] is directly applied to Eq. (2.46):

$$\begin{aligned}
\omega(L, \mu) = & +\frac{1}{3}L - \frac{i}{6}L^0 + \left[ \frac{3\mu^2}{2} + \frac{7}{648} \right] L^{-1} \\
& + \left[ \frac{5i\mu^2}{4} - \frac{137i}{23328} \right] L^{-2} + \left[ \frac{9\mu^4}{8} - \frac{379\mu^2}{432} + \frac{2615}{3779136} \right] L^{-3} \\
& + \left[ \frac{27i\mu^4}{16} - \frac{2677i\mu^2}{5184} + \frac{590983i}{1088391168} \right] L^{-4} \\
& + \left[ \frac{63\mu^6}{16} - \frac{427\mu^4}{576} + \frac{362587\mu^2}{1259712} - \frac{42573661}{117546246144} \right] L^{-5} \\
& + \left[ \frac{333i\mu^6}{32} + \frac{6563i\mu^4}{6912} + \frac{100404965i\mu^2}{725594112} + \frac{11084613257i}{25389989167104} \right] L^{-6}
\end{aligned} \tag{3.50}$$

Our results are summarised in Table I, for which we set  $\ell = 2$  and  $n = 0$  to correspond to the least-damped/longest-lived “fundamental mode” that dominates the QNM signal [6, 7, 32]. We consider backscattering to be negligible. We find that the sixth-order WKB and the Dolan-Ottewill methods are in close agreement. We can ascribe the deviations in the Pöschl-Teller results to the method’s stronger reliance on the potential shape, where the Pöschl-Teller potential is known to match closest to the inverted potential corresponding to a Schwarzschild black hole space-time with a positive cosmological constant [91].

### B. The effect of a mass-like term on the QNF spectrum

From the radial wave equation Eq. (2.46), the characteristic nature of the field is enclosed in the potential; from Eq. (3.48), we observe that the QNF value is strongly influenced by the potential. As such, it is useful to study the QNF spectrum in conjunction with Fig. 1 to understand the effect of the mass-like term. We observe that  $\mu$  elevates the potential: as  $r_*$  increases, the

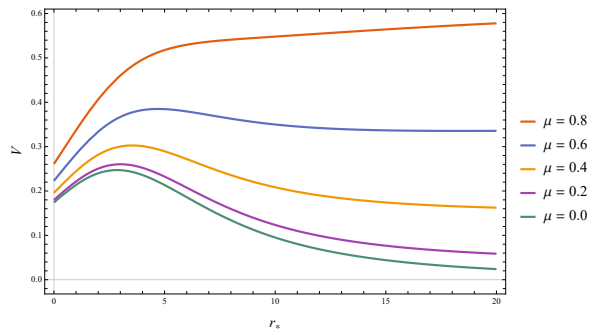


FIG. 1: The  $(n, \ell) = (0, 2)$  mode of the scalar potential of Eq. (2.46) for increasing values of the parameter  $\mu$ . Note that for  $\mu = 0$ ,  $V \rightarrow 0$  as  $r_* \rightarrow \infty$  and the effective potential has a distinct peak. For  $\mu \neq 0$ ,  $V \rightarrow \mu^2$  as  $r_* \rightarrow +\infty$ . When  $\mu^2 \gtrsim V(r_0)$ , the peak is smoothed and the potential barrier is transformed into a potential step.

potential no longer asymptotes to zero but instead approaches  $\mu^2$ . Beyond  $\mu \approx 0.6$ , the peak is smoothed out, suppressing the potential barrier and removing the local maximum.

From Table I demonstrating the fundamental QNM mode, we observe that  $\Re\{\omega\}$  increases steadily with  $\mu$  whereas  $\Im\{\omega\}$  decreases. As  $\mu$  approaches 0.7, there is a discernible change in the QNF behaviour: a large jump in both the real and imaginary parts is observed for all three methods, with a pronounced difference in the WKB result for  $\mu = 0.7$ : a sudden drop in  $\Re\{\omega\}$  and shift from negative to positive in  $\Im\{\omega\}$ . This represents a breakdown in the method: while there is a known increase in the relative error for  $\mu = 0.7$  [19], we observe explicitly from Figure 1 that  $\mu^2 > V(r_0)$  when  $\mu = 0.8$ , which means the use of the WKB method is no longer appropriate.

However, there is also the physical interpretation to consider. In the geodesic picture, we understand that the flattening of the potential forbids the quantum tunnelling that allows the waves to “leak out” from the system. In Ref. [88], massive QNMs for which  $\Re\{\omega^2\} > \mu^2$  are defined as “propagative” and behave similarly to their massless counterparts, whereas  $\Re\{\omega^2\} < \mu^2$  are “evanescent” and contribute negligibly to the QNM spectrum for a perturbed black hole. This shift from propagative to evanescent is characterised by a change in sign in the imaginary part, as observed in Fig. 2. As  $\mu$  increases, the QNMs transition from propagative to evanescent; as the imaginary part goes to zero, the QNMs enter the quasinormal regime [80], where the QNMs are arbitrarily long-lived. In this regime, the ingoing wave amplitude at the event horizon of the black hole is considered much smaller than the amplitude far from the black hole;

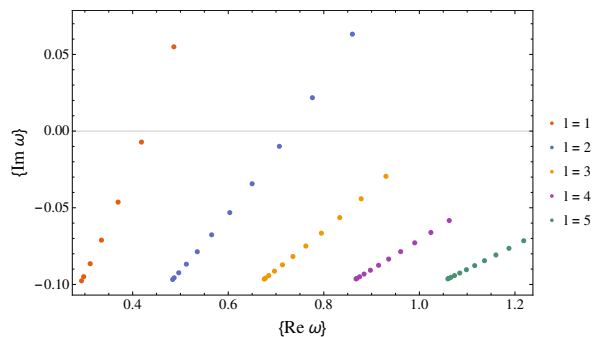


FIG. 2: The QNF spectrum of the extra-dimensional scalar field whose higher-dimensional contribution emerges as a mass-like term. We use the Dolan-Ottewill method to plot the imaginary components against the real for  $\mu \in \{0, 1\}$ . Note that even for these small multipolar numbers, the range of the QNF decreases for increasing  $\ell$ .

since energy no longer “leaks” from the system at spatial infinity, the QNMs behave as standing waves [81].

While we focus on the  $\ell = 2$  mode that dominates the observed QNF spectrum [30, 32], we can see in Figure 2 that the oscillation timescale increases with the angular momentum number. This corresponds well to classical and quantum systems with which we are familiar, where the frequency of an oscillating wave increases with energy. Note, however, that as  $\ell$  increases, the influence of  $\mu$  wanes: the range of the QNF values converge to their massless counterpart for larger multipolar numbers.

In our extra-dimensional setup, the  $\mu$  parameter serves as a manifestation of the extra dimensions. The analysis of the QNM potential and corresponding QNF spectrum conducted here demonstrates that only the “propagative” QNMs can be used as a probe in extra-dimensional searches. This places an upper bound on  $\mu$ , such that  $\Re\{\omega^2\} > \mu^2$ . For a scalar test field in the Schwarzschild black hole space-time, we require that  $\mu < 0.6$ .

### C. An interpretation of $\mu$

Let us begin with considerations from the QNM literature [92], where potentials of the form provided in Eq. (2.46) are studied in the context of massive perturbing fields. We understand  $\mu$  to be of dimensions of inverse length, such that  $m = \mu\hbar$  (under units of  $G = c = 1$ ). The corresponding Compton wavelength  $\lambda_C = h/(mc)$  can then be related to the mass in eV using

$$\lambda_C \times m = 1.24 \times 10^{-9}. \quad (3.51)$$

For Compton wavelengths corresponding to astrophysical black holes (e.g.  $10 M_\odot$  black hole of Schwarzschild radius 30km),  $\mu$  will represent very light particles of mass  $\sim 10^{-10}$  eV [92, 93]. Using the modified dispersion relation of massive-graviton theory, the LVK derived a dynamical lower bound on the graviton Compton wavelength  $\lambda_g \geq 10^{13}$  km at a 90 % confidence, which in turn corresponds to a graviton mass  $m \lesssim 10^{-22}$  eV/c<sup>2</sup> [26]. Since a number of BSM conjectures depend on the existence of light or even ultralight particles (e.g. light scalars of mass  $10^{-32} \leq m \leq 10^{-19}$  eV as in the “string axiverse” scenarios, dark or hidden photons, and other candidates [94]), massive QNMs may be useful in complementary searches for a number of BSM studies.

Of particular importance is the role played by the dimensionless parameter  $M\mu$ , where  $M$  is the ADM black hole mass and  $m = \mu\hbar$  is the bosonic field mass. In the case of spinning black holes, this dimensionless parameter acts as a scaling for the suppression of the instability timescale: when the Compton wavelength of the perturbing field is of the order of the black hole’s radius,  $M\mu \sim 1$  leading to the strongest super-radiant instabilities for the Kerr black hole. This scenario is applicable to light primordial black holes [95] and hypothetical ultralight exotic particles [92].

In our framework, we have positioned the  $\mu$  parameter as an artefact of the extra-dimensional submanifold. To obtain a sense of its magnitude, we revert back to SI units such that the mass of the black hole and the  $\mu$  parameter become

$$M = \frac{Gm^{\text{BH}}}{c^2} \quad \text{and} \quad \mu = \frac{mc}{\hbar}. \quad (3.52)$$

From dimensional analysis, we can show that  $M$  and  $\mu$  have dimensions of length and inverse-length, respectively, such that  $M\mu$  is indeed dimensionless. It is straightforward then that

$$\begin{aligned} M\mu &= \frac{Gm^{\text{BH}}m}{\hbar c} \\ \Rightarrow m &= \frac{1}{m^{\text{BH}}} \frac{\hbar c}{G} M\mu. \end{aligned} \quad (3.53)$$

With the values  $\hbar c/G \sim 10^{-16}$  kg<sup>2</sup>,  $1M_\odot \sim 10^{30}$  kg, and  $M\mu \sim \mathcal{O}(1)$ , we can scale the black hole mass as  $m^{\text{BH}} = 10^x M_\odot$  and thereby express the extra-dimensional contribution through

$$m \sim 10^{-x} 10^{-46} \text{kg} \sim 10^{-(x+10)} \text{eV}/c^2. \quad (3.54)$$

We may use this expression to explore possible mass bounds. From the well-known mass limit for non-evaporating primordial black holes  $M_{PBH} \gtrsim 10^{15}$  g [95],

$m \lesssim 10^{-28}$  kg such that  $\chi \gtrsim -18$ . On the other hand,  $\chi \sim -8$  corresponds to a micro black hole of the same mass as the moon. For the  $62 \pm 4 M_{\odot}$  black hole remnant corresponding to the GW150914 event [34],  $\chi \sim 1$ . Under the proposed higher mass range for supermassive black holes (referred to as “stupendously large black holes”) [96],  $12 \lesssim \chi \lesssim 18$ .

#### IV. CONSTRAINTS FROM GRAVITATIONAL-WAVES

In analogy to the electromagnetic waves produced by accelerating charges, GWs are generated by any massive body undergoing acceleration. This is a direct consequence of the relationship between mass and space-time curvature predicted by GR, where changes in the geometry occur corresponding to the movements of the massive body. Since gravity is weakly-interacting, the resultant ripples in space-time propagate throughout the universe unscreened. This property unlocks unique opportunities for studies into early-universe cosmology, since GWs decouple almost immediately after being produced and then propagate undisturbed throughout the universe; they may be the only way we can probe the time directly after the big bang [49]. However, a consequence of this feeble nature of gravity is a severely limited collection of astrophysical events whose corresponding GW signatures lie within the sensitivity range of detectors. These can be classified into four possible GW sources: coalescing compact bodies, pulsars, supernovae (all of which are sources of *deterministic* GWs), and a *cosmic GW background* comprised of the stochastic GWs emergent in the wake of the big bang [38, 48].

The 90 GW events detected by the LVK collaboration [23] originate from the mergers of compact coalescing binaries, with binary black hole collisions remaining the most common. This is in part due to the energy output during a black hole collision (considered in Ref. [5] as second only to the big bang), as well as the comprehensive understanding of the modelling of these two-body systems [97]. Three distinct phases make up the gravitational waveform:

- (i) inspiral: long, adiabatic stage as orbit shrinks and GW emission increases (post-Newtonian expansion);
- (ii) merger: violent merger into a single black hole and GW emission peaks (numerical relativity simulations);
- (iii) ringdown: final black hole emits damped GWs as it relaxes into a stationary state (black hole pertur-

bation theory).

Parentheses indicate the technique through which each phase is modelled.

Due to the weakly-interacting nature of GWs and the noise in which the signal is saturated, inferring the physical parameters of a GW source is a delicate process dependent on prior knowledge of the expected signal shape and the implementation of several *a priori* assumptions (this is a highly non-trivial exercise, and we refer the interested reader to Ref. [24] for details). However, the observations of GWs from these merger events allow for unique tests of GR within regimes previously beyond reach.

In light of these regular GW detections and the promise of future GW observatories [98–100], interest in using GW data to constrain BSM models is building (see Ref. [38, 49]). However, it is known that GW phenomenology is still in its infancy, unlike collider searches, where we have yet to obtain precise final state signatures for which we can search [40]. This makes it difficult to constrain particle physics models with precision. Methods of searching for new physics predominantly rely on calculating the frequencies associated with symmetry breaking mechanisms to determine whether such signals lie within the sensitivity range of present or future GW detectors – a strategy that long predates the detection of GWs [101–103]. Attempts to place bounds on the size and number of extra dimensions focus on the yet-undetected stochastic GW background rather than those emitted by compact coalescing bodies (see Ref. [40]).

Within the GW community, searches for modified theories of gravity consider how GW signals may differ from those of GR in terms of their generation, propagation, and polarisation [29]. In the case of extra dimensions, it is well understood that additional polarisation states must be considered to describe the extra degrees of freedom. While GR has only two tensor modes (i.e. plus and cross modes), a generalised metric theory of gravity can accommodate up to six polarisation modes: two tensor, two vector, and two scalar modes [104]. However, these can often lie far beyond detectable range e.g. Ref. [43].

For these reasons, we suggest this new avenue of pursuit by which to probe extra dimensions within extant GW data, that exploits the connection between QNM and GW studies. Inspired by tests for deviations from GR within the post-merger phase [28, 29], we make use of one of the few tools dedicated to QNM analyses of GW data: the Python package `PyRING` [32, 105]. The package was recently developed to perform Bayesian parameter estimation, tests of GR, and other QNM analyses through a combination of observed GW data with sim-

TABLE II: To correspond to the search for parametric deviations in GR, we structure our results for  $\omega = \Re\{\omega\}$  and the damping time  $\tau = 1/\Im\{\omega\}$  as  $\omega = \omega^{\mu=0} (1 + \delta\omega)$  and  $\tau = \tau^{\mu=0} (1 + \delta\tau)$ , respectively. We use QNF results provided in column 4 of Table I.

$\mu$	$\omega(\ell, \mu)$	$\delta\omega$	$\delta\tau$
0.0	0.4836 -0.0968i	0.0000	0.0000
0.1	0.4868 -0.0968i	0.0065	0.0113
0.2	0.4963 -0.0924i	0.0262	0.0473
0.3	0.5124 -0.0868i	0.0594	0.1149
0.4	0.5352 -0.0787i	0.1066	0.2302
0.5	0.5653 -0.0676i	0.1687	0.4306
0.6	0.6032 -0.0532i	0.2472	0.8206
0.7	0.6500 -0.0343i	0.3440	1.8181

ulation and numerically-generated waveform templates, following the Bayesian framework detailed in Ref. [24]. Treating GR as the null hypothesis, PYRING tests for deviations from the QNF oscillation frequency ( $\Re\{\omega\} = \omega$ ) and decay timescale ( $1/\Im\{\omega\} = \tau$ ):

$$\begin{aligned}\delta\omega &= \omega^{\text{GR}}(1 + \delta\omega), \\ \delta\tau &= \tau^{\text{GR}}(1 + \delta\tau).\end{aligned}\quad (4.55)$$

As a first exploratory step, we run this agnostic test of GR deviation in GW data from the GW150914 black hole merger event [34] using the provided Kerr<sub>220</sub> waveform template corresponding to the  $\ell = m = 2$ ,  $n = 0$  mode (see Figure 3). The analysis through PYRING is conducted in the time domain using publicly available data from the LVK collaboration [106]. To reduce computational cost, we employ medium-resolution data, simplified noise estimation, and simplified sampler settings, as well as tight priors. Specifically, we follow Ref. [32] in sampling 4096s of data from the Hanford and the Livingston LIGO detectors, sampled at 4096 Hz with the raw strain band-passed over  $f \in [20, 2028]$  Hz before being split into 2-second noise chunks. We set the trigtime in H1 to  $t = 126259462.423227$  s. We run the analysis over the prior bounds for final mass  $M_f \in [50.0, 90.0] M_\odot$ , spin  $a_f \in [0.6, 0.9]$ , amplitude  $A_{220} \in [0.0, 5.0 \times 10^{-20}]$ , and phase  $\phi_{220} \in [0, 2\pi]$ . In testing for deviations from GR, we sample over  $\delta\omega, \delta\tau \in [-1, 1]$ .

To carry out its Bayesian inference, PYRING exploits the nested sampling algorithm of CPNEST [107, 108]. The package's implementation is based on an ensemble Markov chain Monte Carlo (MCMC) sampler, for which we only need to input the specifics of the analysis. We use 2048 live points and set the maximum MCMC steps to 2048, with the default 1234 seeds. At the end of the analysis, we are left with  $\sim 8000$  independent samples and a Bayes factor of  $\ln \mathcal{B} \approx 73.443$ . We visualise these

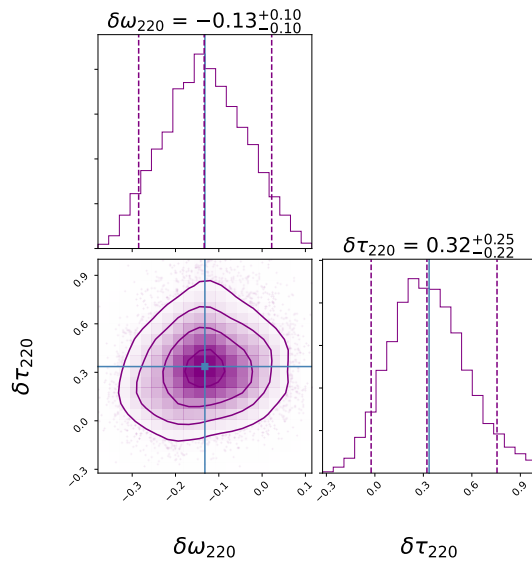


FIG. 3: As a proof-of-concept, we perform a rudimentary parameter estimation of the GR deviations using PYRING for event GW150914 (GW data sampled at 4096 Hz). We narrow priors to reduce computation cost. With CORNER, we plot the 2D posteriors and 1D histograms on  $(\delta\omega, \delta\tau)$ , where  $(0, 0)$  is the GR-predicted value. Dashed lines and contours demarcate the 90% credible region; the blue line indicates the mean.

results in Figure 3.

Higher resolution data diminishes the impact of the time discretisation [33], while increased sampler settings lead to more precise results [107, 108]. For improved accuracy, we therefore make use of the hierarchical combination of LVK's strongest bounds on GR deviations to date [29]:

$$\begin{aligned}\delta\omega_{220} &= 0.02^{+0.07}_{-0.07}, \\ \delta\tau_{220} &= 0.13^{+0.21}_{-0.22}.\end{aligned}\quad (4.56)$$

To compare QNF computation with GW data, we consider our  $\mu = 0$  results to be equivalent to the GR prediction  $(\delta\omega, \delta\tau) = (0, 0)$  i.e.  $\omega^{\text{GR}} = \omega^{\mu=0}$ . From the Dolan-Ottewill results of Table I, we extract the parametric deviations to Table II. We observe that the parametric deviations match the bounds predicted in Eq. (4.56) for  $\mu \sim 0.2$ . If we exploit the QNF series expansion provided in Eq. (3.50), we can solve for  $\mu$  explicitly. In doing so (for the real part and using the dominant  $\ell = 2$ ,  $n = 0$  mode), we find that

$$0.1747 < \mu < 0.3681. \quad (4.57)$$

Since we have set  $M = 1$ , we can interpret this as a bound on the massless parameter  $M\mu$ . If we were considering a massive oscillating field,  $M\mu \sim \mathcal{O}(0.1)$ , and from

Eq. (3.53)  $\chi \sim 3$ , such that the mass of the hypothetical particle is  $m \sim 10^{-13} \text{ eV}/c^2$  for, say, the final  $62M_{\odot}$  black hole remnant of GW150914. This mass corresponds to a light scalar hypothesis rather than the heavier TeV-scale Kaluza-Klein masses of extra-dimensional conjectures [94].

## V. CONCLUSIONS

In this work, we have considered a novel extra-dimensional setup comprised of a Schwarzschild black hole embedded in a 7D product space-time whose extra dimensions form a negative compact space – specifically, a nilmanifold built from Heisenberg algebra. We have pursued a strategy for an extra-dimensional search using QNMs. By positioning the extra-dimensional contribution as an effective mass-like  $\mu^2$  term in the QNM potential, we have demonstrated through a numerical study a possible upper bound on this  $\mu$ . Then, by using searches for parametric deviations from GR, we further constrain this probe. The limits provided in Eq. (4.57) can be interpreted as naïve constraints on the QNM probe into extra dimensions. An open question, however, is to what extent can we apply these constraints to place bounds on the size and number of extra dimensions. For example, a next step could be to subject the mass spectrum of the toy dark matter model studied in Ref. [63] to this result in order to extract tangible bounds on the radius of the nilmanifold extra dimensions herein constructed.

As acknowledged in Ref. [29], there has been substantial progress in GW research from the analytical, numerical, and experimental fronts. GW phenomenology and our ability to perform precision-level testing of GR, however, are still in their infancy. It is our hope that the simple setup we have provided here may be refined as our understanding of the applicability of GW detection in fundamental physics grows, bringing these tests to a new level of accuracy.

## VI. ACKNOWLEDGEMENTS

ASC is supported in part by the National Research Foundation (NRF) of South Africa; AC is supported by the NRF and Department of Science and Innovation through the SA-CERN programme and a Campus France scholarship; EL is supported by the French Government, via École Normale Supérieure de Lyon. AC extends her appreciation to the organisers and participants of the GWOSC Open Data Workshop 2022, which special thanks to those involved in the IP2I study hub hosted by the *groupe Ondes gravitationnelles*.

**Software.** LVK data are interfaced through `GWpy`, with support through `LALSuite`. The publicly-available `pyRing` package can be found at: <https://git.ligo.org/lscsoft/pyring>. We use the `cpnest`: v0.11.4 [108] and `corner`: v2.2.1 [109]. Other open-source python packages required by `pyRing` include `cython` [110], `h5py` [111], `matplotlib` [112], `numpy` [113], `scipy` [114], and `seaborn` [115].

- 
- [1] C. V. Vishveshwara, *Nature* **227**, 936 (1970).
  - [2] W. H. Press, *Astrophys. J. Lett.* **170**, L105 (1971).
  - [3] H.-P. Nollert, *Class. Quant. Grav.* **16**, R159 (1999).
  - [4] K. D. Kokkotas and B. G. Schmidt, *Living Rev. Rel.* **2**, 2 (1999), [arXiv:gr-qc/9909058](https://arxiv.org/abs/gr-qc/9909058).
  - [5] V. Ferrari and L. Gualtieri, *Gen. Rel. Grav.* **40**, 945 (2008), [arXiv:0709.0657](https://arxiv.org/abs/0709.0657) [gr-qc].
  - [6] E. Berti, V. Cardoso, and A. O. Starinets, *Class. Quant. Grav.* **26**, 163001 (2009), [arXiv:0905.2975](https://arxiv.org/abs/0905.2975) [gr-qc].
  - [7] R. A. Konoplya and A. Zhidenko, *Rev. Mod. Phys.* **83**, 793 (2011), [arXiv:1102.4014](https://arxiv.org/abs/1102.4014) [gr-qc].
  - [8] F. Echeverria, *Phys. Rev. D* **40**, 3194 (1989).
  - [9] C. W. Misner, K. S. Thorne, and J. A. Wheeler, *Gravitation* (W. H. Freeman, San Francisco, 1973).
  - [10] W. Israel, *Phys. Rev.* **164**, 1776 (1967).
  - [11] T. Regge and J. A. Wheeler, *Phys. Rev.* **108**, 1063 (1957).
  - [12] F. J. Zerilli, *Phys. Rev. D* **2**, 2141 (1970).
  - [13] G. Pöschl and E. Teller, *Z. Phys.* **83**, 143 (1933).
  - [14] H.-J. Blome and B. Mashhoon, *Physics Letters A* **100**, 231 (1984).
  - [15] B. F. Schutz and C. M. Will, *Astrophys. J.* **291**, L33 (1985).
  - [16] C. M. Will, *Can. J. Phys.* **64**, 140 (1986).
  - [17] S. Iyer and C. M. Will, *Phys. Rev. D* **35**, 3621 (1987).
  - [18] R. A. Konoplya, *Phys. Rev. D* **68**, 024018 (2003), [arXiv:gr-qc/0303052](https://arxiv.org/abs/gr-qc/0303052).
  - [19] R. A. Konoplya, A. Zhidenko, and A. F. Zinhailo, *Class. Quant. Grav.* **36**, 155002 (2019), [arXiv:1904.10333](https://arxiv.org/abs/1904.10333) [gr-qc].
  - [20] S. R. Dolan and A. C. Ottewill, *Class. Quant. Grav.* **26**, 225003 (2009), [arXiv:0908.0329](https://arxiv.org/abs/0908.0329) [gr-qc].
  - [21] C. J. Goebel, *Astrophys. J.* **172** (1972).
  - [22] C.-H. Chen, H.-T. Cho, A. Chrysostomou, and A. S. Cornell, *Phys. Rev. D* **104**, 024009 (2021), [arXiv:2103.07777](https://arxiv.org/abs/2103.07777) [gr-qc].
  - [23] R. Abbott *et al.* (LIGO Scientific, VIRGO, KAGRA), (2021), [arXiv:2111.03606](https://arxiv.org/abs/2111.03606) [gr-qc].

- [24] B. P. Abbott *et al.* (LIGO Scientific, Virgo), *Class. Quant. Grav.* **37**, 055002 (2020), [arXiv:1908.11170 \[gr-qc\]](#).
- [25] C. Van Den Broeck, “Probing dynamical spacetimes with gravitational waves,” in *Springer Handbook of Spacetime*, edited by A. Ashtekar and V. Petkov (Springer, 2014) pp. 589–613.
- [26] B. P. Abbott *et al.* (LIGO Scientific, Virgo), *Phys. Rev. Lett.* **116**, 221101 (2016), [Erratum: *Phys.Rev.Lett.* 121, 129902 (2018)], [arXiv:1602.03841 \[gr-qc\]](#).
- [27] B. P. Abbott *et al.* (LIGO Scientific, Virgo), *Phys. Rev. D* **100**, 104036 (2019), [arXiv:1903.04467 \[gr-qc\]](#).
- [28] R. Abbott *et al.* (LIGO Scientific, Virgo), *Phys. Rev. D* **103**, 122002 (2021), [arXiv:2010.14529 \[gr-qc\]](#).
- [29] R. Abbott *et al.* (LIGO Scientific, VIRGO, KAGRA), (2021), [arXiv:2112.06861 \[gr-qc\]](#).
- [30] E. Berti, V. Cardoso, and C. M. Will, *Phys. Rev. D* **73**, 064030 (2006), [arXiv:gr-qc/0512160](#).
- [31] R. Cotesta, G. Carullo, E. Berti, and V. Cardoso, *Phys. Rev. Lett.* **129**, 111102 (2022), [arXiv:2201.00822 \[gr-qc\]](#).
- [32] G. Carullo, W. Del Pozzo, and J. Veitch, *Phys. Rev. D* **99**, 123029 (2019), [Erratum: *Phys.Rev.D* 100, 089903 (2019)], [arXiv:1902.07527 \[gr-qc\]](#).
- [33] R. Cotesta, G. Carullo, E. Berti, and V. Cardoso, *Phys. Rev. Lett.* **129**, 111102 (2022), [arXiv:2201.00822 \[gr-qc\]](#).
- [34] B. P. Abbott *et al.* (LIGO Scientific, Virgo), *Phys. Rev. Lett.* **116**, 061102 (2016), [arXiv:1602.03837 \[gr-qc\]](#).
- [35] B. P. Abbott *et al.* (LIGO Scientific, Virgo), *Phys. Rev. Lett.* **116**, 241102 (2016), [arXiv:1602.03840 \[gr-qc\]](#).
- [36] D. J. Weir, *Phil. Trans. Roy. Soc. Lond. A* **376**, 20170126 (2018), [arXiv:1705.01783 \[hep-ph\]](#).
- [37] R.-G. Cai, Z. Cao, Z.-K. Guo, S.-J. Wang, and T. Yang, *National Science Review* **4**, 687 (2017), <https://academic.oup.com/nsr/article-pdf/4/5/687/31566614/nwx029.pdf>.
- [38] R. Caldwell *et al.*, (2022), [arXiv:2203.07972 \[gr-qc\]](#).
- [39] W.-C. Huang, F. Sannino, and Z.-W. Wang, *Phys. Rev. D* **102**, 095025 (2020), [arXiv:2004.02332 \[hep-ph\]](#).
- [40] H. Yu, Z.-C. Lin, and Y.-X. Liu, *Commun. Theor. Phys.* **71**, 991 (2019), [arXiv:1905.10614 \[gr-qc\]](#).
- [41] V. Cardoso, L. Gualtieri, and C. J. Moore, *Phys. Rev. D* **100**, 124037 (2019), [arXiv:1910.09557 \[gr-qc\]](#).
- [42] O.-K. Kwon, S. Lee, and D. D. Tolla, *Phys. Rev. D* **100**, 084050 (2019).
- [43] D. Andriot and G. Lucena Gómez, *JCAP* **06**, 048 (2017), [Erratum: *JCAP* 05, E01 (2019)], [arXiv:1704.07392 \[hep-th\]](#).
- [44] Y. Du, S. Tahura, D. Vaman, and K. Yagi, *Phys. Rev. D* **103**, 044031 (2021).
- [45] C. Ferko, G. Satishchandran, and S. Sethi, *Phys. Rev. D* **105**, 024072 (2022).
- [46] D. Andriot and D. Tsimpis, *JHEP* **06**, 100 (2020), [arXiv:1911.01444 \[hep-th\]](#).
- [47] D. Andriot, P. Marconnet, and D. Tsimpis, *JCAP* **07**, 040 (2021), [arXiv:2103.09240 \[hep-th\]](#).
- [48] M. Bailes *et al.*, *Nature Rev. Phys.* **3**, 344 (2021).
- [49] N. Aggarwal *et al.*, *Living Rev. Rel.* **24**, 4 (2021), [arXiv:2011.12414 \[gr-qc\]](#).
- [50] L. Randall and R. Sundrum, *Phys. Rev. Lett.* **83**, 4690 (1999), [arXiv:hep-th/9906064](#).
- [51] T. Shiromizu, K.-i. Maeda, and M. Sasaki, *Phys. Rev. D* **62**, 024012 (2000), [arXiv:gr-qc/9910076](#).
- [52] A. K. Mishra, A. Ghosh, and S. Chakraborty, (2021), [arXiv:2106.05558 \[gr-qc\]](#).
- [53] T. Needham, *Visual complex analysis* (Clarendon Press, 2012).
- [54] M. Berger, *A Panoramic View of Riemannian Geometry* (Springer Berlin, 2013).
- [55] S. S. Haque, G. Shiu, B. Underwood, and T. Van Riet, *Phys. Rev. D* **79**, 086005 (2009), [arXiv:0810.5328 \[hep-th\]](#).
- [56] D. Andriot and J. Blåbäck, *JHEP* **03**, 102 (2017), [Erratum: *JHEP* 03, 083 (2018)], [arXiv:1609.00385 \[hep-th\]](#).
- [57] D. Andriot, L. Horer, and P. Marconnet, *JHEP* **06**, 131 (2022), [arXiv:2201.04152 \[hep-th\]](#).
- [58] G. D. Starkman, D. Stojkovic, and M. Trodden, *Phys. Rev. Lett.* **87**, 231303 (2001), [arXiv:hep-th/0106143](#).
- [59] C.-M. Chen, P.-M. Ho, I. P. Neupane, N. Ohta, and J. E. Wang, *JHEP* **10**, 058 (2003), [arXiv:hep-th/0306291](#).
- [60] I. P. Neupane, *Class. Quant. Grav.* **21**, 4383 (2004), [arXiv:hep-th/0311071](#).
- [61] D. Orlando and S. C. Park, *JHEP* **08**, 006 (2010), [arXiv:1006.1901 \[hep-th\]](#).
- [62] L. Randall and R. Sundrum, *Phys. Rev. Lett.* **83**, 3370 (1999), [arXiv:hep-ph/9905221](#).
- [63] D. Andriot, G. Cacciapaglia, A. Deandrea, N. Deutschmann, and D. Tsimpis, *JHEP* **06**, 169 (2016), [arXiv:1603.02289 \[hep-th\]](#).
- [64] D. Andriot and D. Tsimpis, *JHEP* **09**, 096 (2018), [arXiv:1806.05156 \[hep-th\]](#).
- [65] D. Andriot, A. Cornell, A. Deandrea, F. Dogliotti, and D. Tsimpis, *JHEP* **05**, 122 (2020), [arXiv:2002.11128 \[hep-th\]](#).
- [66] A. Deandrea, F. Dogliotti, and D. Tsimpis, *Phys. Lett. B* **829**, 137097 (2022), [arXiv:2201.01151 \[hep-ph\]](#).
- [67] A. Deandrea, F. Dogliotti, and D. Tsimpis, *Nucl. Phys. B* **982**, 115895 (2022), [arXiv:2202.11437 \[hep-th\]](#).
- [68] D. Andriot, *JHEP* **02**, 112 (2016), [arXiv:1507.00014 \[hep-th\]](#).
- [69] C. Bock, *Asian Journal of Mathematics* **20**, 199 (2016), [arXiv:0903.2926 \[math.DG\]](#).
- [70] M. Grana, R. Minasian, M. Petrini, and A. Tomasiello, *JHEP* **05**, 031 (2007), [arXiv:hep-th/0609124](#).
- [71] D. Andriot, *String theory flux vacua on twisted tori and Generalized Complex Geometry*, Ph.D. thesis, Paris U., VI-VII (2010).
- [72] A. I. Malcev, *Amer. Math. Soc. Translation* **39** (1951).
- [73] S. Thangavelu, *Revista de la Union Matematica Argentina* **50**, 71 (2009).
- [74] J. D. Bekenstein, *Contemp. Phys.* **45**, 31 (2003), [arXiv:quant-ph/0311049](#).
- [75] S. Chandrasekhar, *The Mathematical Theory of Black Holes* (Oxford University Press, New York, 1983).

- [76] S. W. Hawking, *Commun. Math. Phys.* **43**, 199 (1975), [Erratum: *Commun.Math.Phys.* 46, 206 (1976)].
- [77] W. Barreto, A. Da Silva, R. Gomez, L. Lehner, L. Rosales, and J. Winicour, *Phys. Rev. D* **71**, 064028 (2005), [arXiv:gr-qc/0412066](#).
- [78] H. Yoshino, T. Shiromizu, and M. Shibata, *Phys. Rev. D* **74**, 124022 (2006), [arXiv:gr-qc/0610110](#).
- [79] L. E. Simone and C. M. Will, *Class. Quant. Grav.* **9**, 963 (1992).
- [80] A. Ohashi and M.-a. Sakagami, *Class. Quant. Grav.* **21**, 3973 (2004), [arXiv:gr-qc/0407009](#).
- [81] R. A. Konoplya and A. V. Zhidenko, *Phys. Lett. B* **609**, 377 (2005), [arXiv:gr-qc/0411059](#).
- [82] S. R. Dolan, *Phys. Rev. D* **76**, 084001 (2007), [arXiv:0705.2880 \[gr-qc\]](#).
- [83] J. G. Rosa and S. R. Dolan, *Phys. Rev. D* **85**, 044043 (2012), [arXiv:1110.4494 \[hep-th\]](#).
- [84] B. C. Seymour and K. Yagi, *Classical and Quantum Gravity* **37**, 145008 (2020).
- [85] V. Ferrari and B. Mashhoon, *Phys. Rev. D* **30**, 295 (1984).
- [86] V. Ferrari and B. Mashhoon, *Phys. Rev. Lett.* **52**, 1361 (1984).
- [87] N. Fröman and P. O. Fröman, *JWKB Approximation: Contributions to the Theory*, 1st ed. (North-Holland, Amsterdam, 1965).
- [88] J. Percival and S. R. Dolan, *Phys. Rev. D* **102**, 104055 (2020), [arXiv:2008.10621 \[gr-qc\]](#).
- [89] J. Matyjasek and M. Opala, *Phys. Rev. D* **96**, 024011 (2017).
- [90] J. Matyjasek and M. Telecka, *Phys. Rev. D* **100**, 124006 (2019).
- [91] A. Zhidenko, *Class. Quantum Gravity* **21**, 273 (2004).
- [92] E. Berti (2014) [arXiv:1410.4481 \[gr-qc\]](#).
- [93] M. Lagos, P. G. Ferreira, and O. J. Tattersall, *Phys. Rev. D* **101**, 084018 (2020), [arXiv:2002.01897 \[gr-qc\]](#).
- [94] R. L. Workman and Others (Particle Data Group), *PTEP* **2022**, 083C01 (2022).
- [95] M. Sasaki, T. Suyama, T. Tanaka, and S. Yokoyama, *Class. Quant. Grav.* **35**, 063001 (2018), [arXiv:1801.05235 \[astro-ph.CO\]](#).
- [96] B. Carr, F. Kuhnel, and L. Visinelli, *Mon. Not. Roy. Astron. Soc.* **501**, 2029 (2021), [arXiv:2008.08077 \[astro-ph.CO\]](#).
- [97] P. Jaranowski and A. Krolak, *Living Rev. Rel.* **8**, 3 (2005), [arXiv:0711.1115 \[gr-qc\]](#).
- [98] C. S. Unnikrishnan, *Int. J. Mod. Phys. D* **22**, 1341010 (2013).
- [99] P. Amaro-Seoane *et al.*, *Class. Quant. Grav.* **29**, 124016 (2012).
- [100] D. Reitze *et al.*, *Bull. Am. Astron. Soc.* **51**, 035 (2019).
- [101] C. M. Will, *Phys. Rev. D* **57**, 2061 (1998), [arXiv:gr-qc/9709011](#).
- [102] C. J. Hogan, *Phys. Rev. Lett.* **85**, 2044 (2000).
- [103] C. J. Hogan, *Phys. Rev. D* **62**, 121302 (2000), [arXiv:astro-ph/0009136](#).
- [104] D. M. Eardley, D. L. Lee, A. P. Lightman, R. V. Wagoner, and C. M. Will, *Phys. Rev. Lett.* **30**, 884 (1973).
- [105] M. Isi, M. Giesler, W. M. Farr, M. A. Scheel, and S. A. Teukolsky, *Phys. Rev. Lett.* **123**, 111102 (2019), [arXiv:1905.00869 \[gr-qc\]](#).
- [106] R. Abbott *et al.* (LIGO Scientific, Virgo), *SoftwareX* **13**, 100658 (2021), [arXiv:1912.11716 \[gr-qc\]](#).
- [107] J. Veitch and A. Vecchio, *Phys. Rev. D* **81**, 062003 (2010), [arXiv:0911.3820 \[astro-ph.CO\]](#).
- [108] J. Veitch, W. D. Pozzo, A. Lyttle, M. J. Williams, C. Talbot, M. Pitkin, G. Ashton, Cody, M. Hübner, A. Nitz, D. Mihaylov, D. Macleod, G. Carullo, G. Davies, and ttw, “[johnveitch/cpnest: v0.11.4](#),” (2022).
- [109] D. Foreman-Mackey, *The Journal of Open Source Software* **1**, 24 (2016).
- [110] S. Behnel, R. Bradshaw, C. Citro, L. Dalcin, D. S. Seljebotn, and K. Smith, *Computing in Science & Engineering* **13**, 31 (2011).
- [111] A. Collette, *Python and HDF5* (O’Reilly, 2013).
- [112] J. D. Hunter, *Computing in Science & Engineering* **9**, 90 (2007).
- [113] C. R. Harris, K. J. Millman, S. J. van der Walt, R. Gommers, P. Virtanen, D. Cournapeau, E. Wieser, J. Taylor, S. Berg, N. J. Smith, R. Kern, M. Picus, S. Hoyer, M. H. van Kerkwijk, M. Brett, A. Haldane, J. F. del Río, M. Wiebe, P. Peterson, P. Gérard-Marchant, K. Sheppard, T. Reddy, W. Weckesser, H. Abbasi, C. Gohlke, and T. E. Oliphant, *Nature* **585**, 357 (2020).
- [114] P. Virtanen, R. Gommers, T. E. Oliphant, M. Haberland, T. Reddy, D. Cournapeau, E. Burovski, P. Peterson, W. Weckesser, J. Bright, S. J. van der Walt, M. Brett, J. Wilson, K. J. Millman, N. Mayorov, A. R. J. Nelson, E. Jones, R. Kern, E. Larson, C. J. Carey, Í. Polat, Y. Feng, E. W. Moore, J. VanderPlas, D. Laxalde, J. Perktold, R. Cimrman, I. Henriksen, E. A. Quintero, C. R. Harris, A. M. Archibald, A. H. Ribeiro, F. Pedregosa, P. van Mulbregt, and SciPy 1.0 Contributors, *Nature Methods* **17**, 261 (2020).
- [115] M. L. Waskom, *Journal of Open Source Software* **6**, 3021 (2021).